14 LASER RESONATORS

14.1 INTRODUCTION

Until now we have supposed a laser resonator to consist of two highly reflecting, flat, parallel mirrors separated by some distance L. The only important property of such a resonator for our purposes thus far is that it has "longitudinal" modes separated in frequency by $c/2L$. We have not concerned ourselves with how the field inside the resonator varies in directions transverse to the line joining the centers of the mirrors. In fact we have assumed the field to be uniform in any plane perpendicular to this so-called optical axis. In this chapter we will consider laser resonators more realistically. We will consider some of the important characteristics of actual laser resonators, beginning with a rather simple approach based on geometrical optics, and gradually working our way up to a description based on Maxwell's equations.

Most of our treatment of laser resonators will assume that the laser medium is *passive*. That is, the electromagnetic modes of the laser resonator will be assumed to be the same as the modes of an *empty* resonator having no gain medium. This is a good approximation if the gain coefficient and refractive index of the medium are fairly uniform throughout the medium. This is obviously a useful approximation, because it allows us to consider laser resonators independently of the laser medium. Fortunately it is often an accurate approximation.

Figure 14.1*a* shows a light ray normal to the mirrors of a resonator with flat, parallel mirrors. The ray keeps retracing its path on successive reflections from the mirrors. If the mirrors are not perfectly parallel, however, the ray will eventually escape from the resonator, as indicated in Figure 14.1*b*. The misaligned resonator of Figure 14.1*b* requires greater gain for laser oscillation than the resonator of Figure 14.1*a*. We might find, for instance, that a laser with flat mirrors turns off

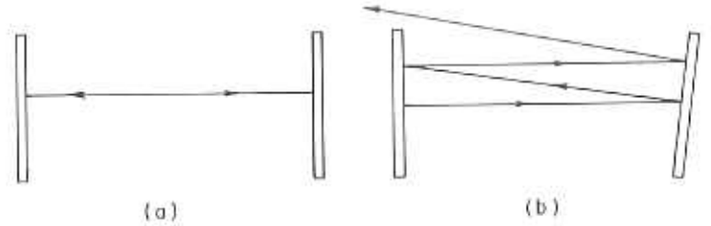

Figure 14.1 A laser resonator with flat, parallel mirrors. A light ray parallel to the optical axis remains inside the resonator if the mirrors are perfectly parallel (*a*). Otherwise it eventually escapes (*b*).

Figure 14.2 A laser resonator with mirrors that are spherical surfaces with radii of curvature R_1 and R_2.

(i.e., laser action ceases) at the slightest misalignment of the mirrors. Obviously this is undesirable if we wish to construct a practical and durable laser. Figure 14.2 shows a much more commonly used type of laser resonator, consisting of mirrors with spherical surfaces. This is the type of resonator used in most commercially available lasers. In Section 14.3 we will see why.

14.2 THE RAY MATRIX

In geometrical optics light propagation is described in terms of rays. We may define a ray at each point on a wave as an arrow drawn normal to the wave front. (Figure 14.3). We will assume that the direction of a ray is the direction of energy flow. There is no physical significance to the "length" of a ray: a ray merely represents a direction of propagation at a given point. When we adopt this ray picture we are ignoring the polarization of the light waves. Our ray picture is a crude but useful representation of the actual physical situation.

In this section we will develop a convenient formalism for ray propagation. This formalism will turn out to be appropriate for the description of *Gaussian* laser beams, which are discussed in Section 14.5.

In situations of practical interest we are dealing with light waves traveling more or less in a single direction, which we will call the z direction. The rays we envision point almost parallel to the z axis. At any point on the wave we imagine a ray having a lateral displacement $r(z)$, measured from the z axis, and a slope (Figure 14.4)

$$r'(z) = \frac{dr}{dz} \tag{14.2.1}$$

Because of our assumption of nearly unidirectional propagation along z, the slope $r'(z)$ of a ray will be very small, so that (Figure 14.4)

$$r'(z) = \tan\theta \approx \sin\theta \approx \theta \tag{14.2.2}$$

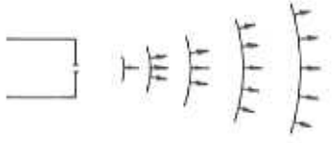

Figure 14.3 Rays drawn on a wave represent the direction of propagation.

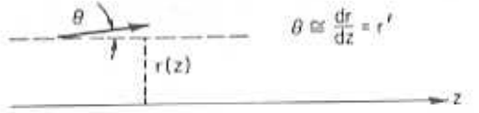

Figure 14.4 A ray is characterized by its displacement r and slope r' measured from some z axis.

Such rays are called *paraxial rays*. We will assume, as is implicit in our definition of the ray displacement r and slope r', that we have cylindrical symmetry about the z axis. The slope of a ray is taken to be positive or negative depending whether the displacement r is increasing or decreasing in the direction of propagation.

We would like to relate the displacement and slope of a ray at a point z to the displacement and slope at a point z'. Consider, for example, the simple case of vacuum propagation from z_1 to z_2. In vacuum there is nothing to change the direction of a ray, so we have (Figure 14.5):

$$r(z_2) = r(z_1) + r'(z_1)(z_2 - z_1) \tag{14.2.3}$$

and

$$r'(z_2) = r'(z_1) \tag{14.2.4}$$

In matrix notation we may write Eqs. (14.2.3) and (14.2.4) as

$$\begin{bmatrix} r(z_2) \\ r'(z_2) \end{bmatrix} = \begin{bmatrix} 1 & z_2 - z_1 \\ 0 & 1 \end{bmatrix} \begin{bmatrix} r(z_1) \\ r'(z_1) \end{bmatrix} \tag{14.2.5}$$

A ray is completely characterized by the 2×1 matrix, or *column vector*,

$$\begin{bmatrix} r \\ r' \end{bmatrix}$$

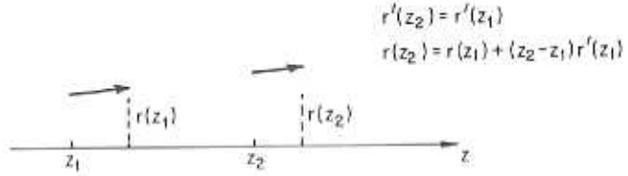

Figure 14.5 The transformation of a ray as a result of free propagation over a distance $z_2 - z_1$.

and Eq. (14.2.5) relates the *final ray*

$$\begin{bmatrix} r_f \\ r_f' \end{bmatrix} = \begin{bmatrix} r(z_2) \\ r'(z_2) \end{bmatrix} \tag{14.2.6}$$

to the *initial ray*

$$\begin{bmatrix} r_i \\ r_i' \end{bmatrix} = \begin{bmatrix} r(z_1) \\ r'(z_1) \end{bmatrix} \tag{14.2.7}$$

Thus, according to Eq. (14.2.5), the vacuum propagation of a ray through a distance $d = z_2 - z_1$ is described by the matrix equation

$$\begin{bmatrix} r_f \\ r_f' \end{bmatrix} = \begin{bmatrix} 1 & d \\ 0 & 1 \end{bmatrix} \begin{bmatrix} r_i \\ r_i' \end{bmatrix} \tag{14.2.8}$$

Given the initial ray with displacement r_i and slope r_i', this equation tells us how that ray is modified by propagation through a distance d.

Consider next the more interesting example of the transformation of a (paraxial) ray by a thin lens of focal length f (Figure 14.6). Immediately to the right of the lens the ray's lateral displacement r_f is the same as the initial displacement r_i immediately to the left:

$$r_f = r_i \tag{14.2.9}$$

The slope of the ray, however, is changed by the lens. From the thin lens equation relating the object and image distances with the focal length of the lens, we obtain (Figure 14.6)

$$r_f' = r_i' - \frac{r_i}{f} \tag{14.2.10}$$

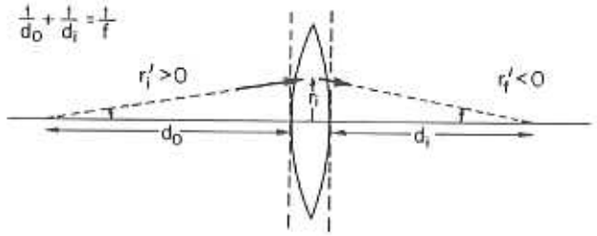

Figure 14.6 Ray transformation by a thin lens.

In matrix notation, Eqs. (14.2.9) and (14.2.10) take the form

$$\begin{bmatrix} r_f \\ r_f' \end{bmatrix} = \begin{bmatrix} 1 & 0 \\ -1/f & 1 \end{bmatrix} \begin{bmatrix} r_i \\ r_i' \end{bmatrix} \tag{14.2.11}$$

One more example will be of interest to us, namely, the case of a spherical mirror with radius of curvature R. The displacement of the ray is the same immediately before and after reflection from the mirror, i.e., $r_f = r_i$. The slope of the ray after reflection, however, is (Figure 14.7)

$$r_f' = r_i' - \frac{2r_i}{R} \tag{14.2.12}$$

In matrix notation, therefore, the ray transformation by the spherical mirror is given by the equation

$$\begin{bmatrix} r_f \\ r_f' \end{bmatrix} = \begin{bmatrix} 1 & 0 \\ -2/R & 1 \end{bmatrix} \begin{bmatrix} r_i \\ r_i' \end{bmatrix} \tag{14.2.13}$$

There is a sign convention for r', namely, $r' > 0$ if r is increasing with propagation, $r' < 0$ otherwise. With this in mind, our sign convention for the radius of curvature R of a spherical mirror is easily checked: R is positive for a concave mirror (Figure 14.7) and negative for a convex mirror. Similarly the focal length f of a lens is positive for a converging lens (Figure 14.6) and negative for a diverging lens. These statements may be verified by making sketches like those in Figures 14.6 and 14.7. Thus (14.2.11) and (14.2.13) apply also to diverging lenses

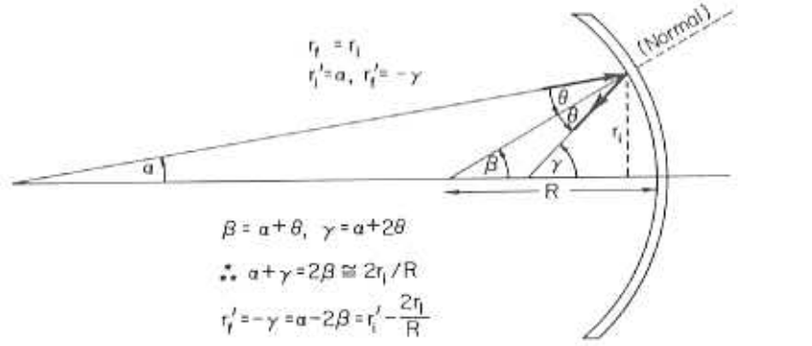

Figure 14.7 Paraxial ray transformation by a spherical mirror surface with radius of curvature R. The relation between r_f' and r_i' is obtained by applying the trigonometric theorem that an exterior angle of a triangle equals the sum of the two opposite interior angles, and the approximation $\beta \approx 2r_i/R$ that holds for paraxial rays.

and convex mirrors, respectively, provided f and R are taken to be negative in those cases.

We have considered thus far the transformation of a ray by three different "optical elements"—empty space of length d, a thin lens of focal length f, and a spherical mirror of radius of curvature R. In general an optical element will transform a ray according to the matrix equation

$$\begin{bmatrix} r_f \\ r_f' \end{bmatrix} = \begin{bmatrix} A & B \\ C & D \end{bmatrix} \begin{bmatrix} r_i \\ r_i' \end{bmatrix} \tag{14.2.14}$$

The 2×2 matrix on the right-hand side of this equation is called the *ray matrix*, or *ABCD* matrix, for the optical element. Equations (14.2.8), (14.2.11), and (14.2.13) give the ray matrices for a straight section of length d, a thin lens of focal length f, and a spherical mirror of radius of curvature R, respectively.

Let us consider the effect on a ray of an open path section of length d followed by a thin lens of focal length f. If a ray has displacement r_i and slope r_i' initially, then after the open section of propagation it has displacement r and slope r' given by Eq. (14.2.8):

$$\begin{bmatrix} r \\ r' \end{bmatrix} = \begin{bmatrix} 1 & d \\ 0 & 1 \end{bmatrix} \begin{bmatrix} r_i \\ r_i' \end{bmatrix} \tag{14.2.15}$$

This gives the "initial" ray displacement and slope immediately before passage through the lens. The "final" ray displacement and slope are therefore given by Eq. (14.2.11):

$$\begin{aligned} \begin{bmatrix} r_f \\ r_f' \end{bmatrix} &= \begin{bmatrix} 1 & 0 \\ -1/f & 1 \end{bmatrix} \begin{bmatrix} r \\ r' \end{bmatrix} \\ &= \begin{bmatrix} 1 & 0 \\ -1/f & 1 \end{bmatrix} \begin{bmatrix} 1 & d \\ 0 & 1 \end{bmatrix} \begin{bmatrix} r_i \\ r_i' \end{bmatrix} \\ &= \begin{bmatrix} 1 & d \\ -1/f & 1 - d/f \end{bmatrix} \begin{bmatrix} r_i \\ r_i' \end{bmatrix} \end{aligned} \tag{14.2.16}$$

The matrix

$$\begin{bmatrix} 1 & d \\ -1/f & 1 - d/f \end{bmatrix} = \begin{bmatrix} 1 & 0 \\ -1/f & 1 \end{bmatrix} \begin{bmatrix} 1 & d \\ 0 & 1 \end{bmatrix} \tag{14.2.17}$$

is therefore the ray matrix for the combined optical system consisting of an open section of length d followed by a thin lens of focal length f. It is the product of the ray matrices for an open section and a lens. It follows that if we have any number of optical elements in some sequence, then the ray matrix for the system comprising all these elements is the matrix product of the ray matrices of the individual elements. Since the matrix product $M_1 M_2$ is in general not the same as $M_2 M_1$, the order of the matrices in the product is important. Thus the system ray matrix is the ray matrix of the first optical element encountered, multiplied *on the left* by the ray matrix of the second optical element, multiplied *on the left* by the ray matrix of the third element, etc. The reader may easily show, for instance, that the ray matrix for the system consisting of an open section followed by a thin lens is different from the ray matrix for a thin lens followed by an open section (Problem 14.1). This means, of course, that the effects of the two systems on a ray are different.

14.3 RESONATOR STABILITY

One of the simplest but most important questions concerning a laser resonator is whether it is *stable*. To see what this means, consider an arbitrary (paraxial) ray bouncing back and forth between the mirrors of a resonator. If the ray remains within the resonator, the resonator is said to be stable. If, however, the ray escapes from the resonator after a sufficiently large number of reflections, the resonator is unstable. Figure 14.1*b*, for example, shows that a misaligned flat-mirror resonator is unstable. In general a stability criterion for a laser resonator can be expressed in terms of the radii of curvature of the mirrors and the distance separating the mirrors. We will now derive this stability criterion with the aid of the *ABCD* matrix.

Consider the resonator sketched in Figure 14.2, consisting of mirrors of radii of curvature R_1 and R_2, separated by a distance L. As drawn, the mirrors are concave. Our analysis, however, will apply also to the case of convex mirrors if we recall that a convex mirror by convention has a negative radius of curvature. We note also that a flat mirror may be regarded as a spherical mirror surface with an infinite radius of curvature.

Imagine a ray starting at the left mirror of Figure 14.2. After a round trip through the resonator, this ray will have been transformed by a straight section of length L, a spherical mirror of radius of curvature R_2, another straight section of length L, and finally a spherical mirror of radius of curvature R_1. The ray matrix describing the ray transformation by a round trip through the resonator is

$$\begin{aligned} \begin{bmatrix} A & B \\ C & D \end{bmatrix} &= \begin{bmatrix} 1 & 0 \\ -2/R_1 & 1 \end{bmatrix} \begin{bmatrix} 1 & L \\ 0 & 1 \end{bmatrix} \begin{bmatrix} 1 & 0 \\ -2/R_2 & 1 \end{bmatrix} \begin{bmatrix} 1 & L \\ 0 & 1 \end{bmatrix} \\ &= \begin{bmatrix} 1 - \dfrac{2L}{R_2} & 2L - \dfrac{2L^2}{R_2} \\ \dfrac{4L}{R_1 R_2} - \dfrac{2}{R_1} - \dfrac{2}{R_2} & 1 - \dfrac{2L}{R_2} - \dfrac{4L}{R_1} + \dfrac{4L^2}{R_1 R_2} \end{bmatrix} \end{aligned} \tag{14.3.1}$$

After N round trips through the resonator, therefore, the initial ray with displacement r_i and slope r_i' is transformed to the ray with displacement r_N and slope r_N' given by

$$\begin{bmatrix} r_N \\ r_N' \end{bmatrix} = \begin{bmatrix} A & B \\ C & D \end{bmatrix}^N \begin{bmatrix} r_i \\ r_i' \end{bmatrix} \tag{14.3.2}$$

where the ray $(ABCD)$ matrix is defined by (14.3.1). The ray matrix (14.3.1) has determinant[1]

$$AD - BC = 1 \tag{14.3.3}$$

Using this fact, and defining an angle θ by

$$\cos\theta = \tfrac{1}{2}(A + D) \tag{14.3.4}$$

it may be shown (see below) that

$$\begin{bmatrix} A & B \\ C & D \end{bmatrix}^N = \frac{1}{\sin\theta} \begin{bmatrix} A\sin N\theta - \sin(N-1)\theta & B\sin N\theta \\ C\sin N\theta & D\sin N\theta - \sin(N-1)\theta \end{bmatrix} \tag{14.3.5}$$

• The result (14.3.5) for a 2×2 matrix satisfying (14.3.3) is sometimes called "Sylvester's theorem." It may be proved by induction: it obviously holds for the case $N = 1$, and so we try to show that if it holds for a single given (but arbitrary) N it must hold also for $N + 1$. If we can show this, Sylvester's theorem is proved.

Thus let us assume that (14.3.5) holds, so that

$$\begin{aligned} \begin{bmatrix} A & B \\ C & D \end{bmatrix}^{N+1} &= \begin{bmatrix} A & B \\ C & D \end{bmatrix} \begin{bmatrix} A & B \\ C & D \end{bmatrix}^N \\ &= \frac{1}{\sin\theta} \begin{bmatrix} A & B \\ C & D \end{bmatrix} \begin{bmatrix} A\sin N\theta - \sin(N-1)\theta & B\sin N\theta \\ C\sin N\theta & D\sin N\theta - \sin(N-1)\theta \end{bmatrix} \\ &= \frac{1}{\sin\theta} \begin{bmatrix} (A^2 + BC)\sin N\theta - A\sin(N-1)\theta & B(A+D)\sin N\theta - B\sin(N-1)\theta \\ C(A+D)\sin N\theta - C\sin(N-1)\theta & (BC + D^2)\sin N\theta - D\sin(N-1)\theta \end{bmatrix} \end{aligned} \tag{14.3.6}$$

1. The simplest way to check this is to note that the ray matrix (14.3.1) is a product of four matrices, each having determinant equal to one. Since the determinant of the product of matrices is equal to the product of the determinants, (14.3.3) follows.

Using (14.3.3) and (14.3.4), we see that the (1, 1) element of this matrix is

$$\begin{aligned} &(A^2 + BC)\sin N\theta - A\sin(N-1)\theta \\ &\quad = (A^2 + AD - 1)\sin N\theta - A\sin(N-1)\theta \\ &\quad = A(A+D)\sin N\theta - \sin N\theta - A\sin(N-1)\theta \\ &\quad = 2A\sin N\theta\cos\theta - \sin N\theta - A\sin(N-1)\theta \\ &\quad = 2A\left[\tfrac{1}{2}\sin(N+1)\theta + \tfrac{1}{2}\sin(N-1)\theta\right] - \sin N\theta - A\sin(N-1)\theta \\ &\quad = A\sin(N+1)\theta - \sin N\theta \end{aligned} \tag{14.3.7}$$

The remaining three matrix elements of (14.3.6) may be evaluated similarly. We obtain

$$\begin{bmatrix} A & B \\ C & D \end{bmatrix}^{N+1} = \frac{1}{\sin\theta} \begin{bmatrix} A\sin(N+1)\theta - \sin N\theta & B\sin(N+1)\theta \\ C\sin(N+1)\theta & D\sin(N+1)\theta - \sin N\theta \end{bmatrix} \tag{14.3.8}$$

But this is just Eq. (14.3.5) with N replaced by $N + 1$. Thus (14.3.5) is true for $N = 1$, and we have just shown that if it is true for any N, then it must be true also for $N + 1$. This proves Sylvester's theorem. •

It now follows from Eq. (14.3.2) that

$$\begin{bmatrix} r_N \\ r_N' \end{bmatrix} = \frac{1}{\sin\theta} \begin{bmatrix} A\sin N\theta - \sin(N-1)\theta & B\sin N\theta \\ C\sin N\theta & D\sin N\theta - \sin(N-1)\theta \end{bmatrix} \begin{bmatrix} r_i \\ r_i' \end{bmatrix} \tag{14.3.9}$$

where, from (14.3.4) and (14.3.1),

$$\begin{aligned} \cos\theta &= \frac{1}{2}\left(1 - \frac{2L}{R_2} + 1 - \frac{2L}{R_2} - \frac{4L}{R_1} + \frac{4L^2}{R_1R_2}\right) \\ &= 1 - \frac{2L}{R_1} - \frac{2L}{R_2} + \frac{2L^2}{R_1R_2} \end{aligned} \tag{14.3.10}$$

Equation (14.3.9) gives the ray displacement and slope after N round trips through the resonator. We observe that r_N (and r_N') stays finite as long as θ is real. If θ is a complex number, however, then $\sin N\theta = (e^{iN\theta} - e^{-iN\theta})/2i$ can be very large for large N, and in fact diverges as $N \to \infty$. In other words, if θ is not purely real, r_N itself will diverge, i.e., the ray will escape from the confines of the resonator. Thus the condition for resonator stability is for θ to be real, which means that $|\cos\theta| \leq 1$, or, from (14.3.10),

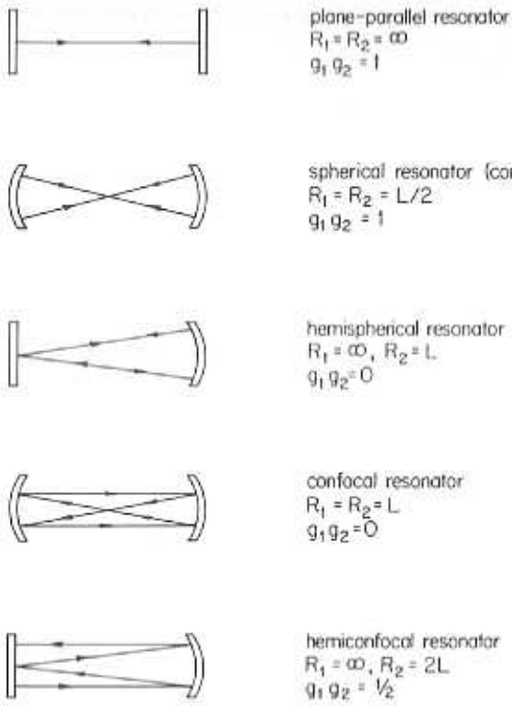

Figure 14.8 Examples of stable resonators.

$$-1 \leqq 1 - \frac{2L}{R_1} - \frac{2L}{R_2} + \frac{2L^2}{R_1 R_2} \leqq 1$$

$$-2 \leqq -\frac{2L}{R_1} - \frac{2L}{R_2} + \frac{2L^2}{R_1 R_2} \leqq 0$$

$$0 \leqq 1 - \frac{L}{R_1} - \frac{L}{R_2} + \frac{L^2}{R_1 R_2} \leqq 1 \qquad (14.3.11)$$

This stability condition is usually written in the laser literature as

$$0 \leqq g_1 g_2 \leqq 1 \qquad (14.3.12)$$

where

$$g_1 = 1 - \frac{L}{R_1} \qquad (14.3.13a)$$

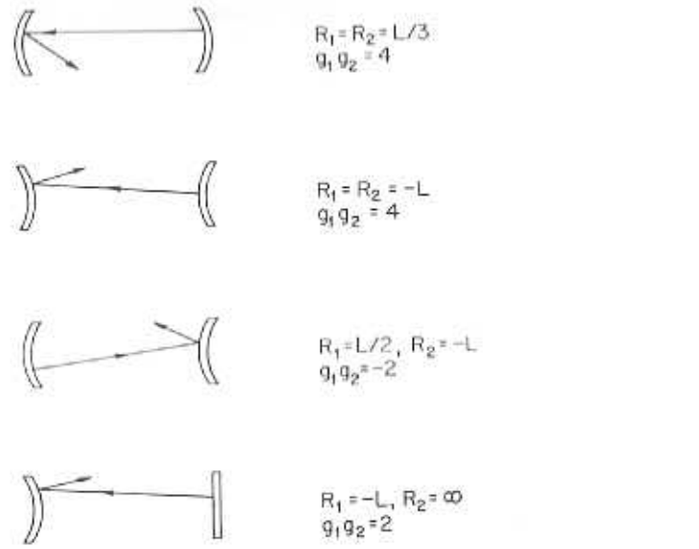

Figure 14.9 Examples of unstable resonators.

and

$$g_2 = 1 - \frac{L}{R_2} \qquad (14.3.13b)$$

These are called the *g parameters* of the resonator. If the g parameters are such that (14.3.12) is satisfied, the resonator is stable. If $g_1 g_2 < 0$ or $g_1 g_2 > 1$, however, the resonator is unstable.

The ray-matrix approach allows us to check immediately whether a given resonator is stable, without having to perform a ray trace such as that shown in Figure 14.1*b*. Whether a given resonator is stable or unstable depends only on the radii of curvature of the mirrors and the distance separating them. Figures 14.8 and 14.9 show examples of stable and unstable resonators, respectively. The reader may easily check in each case whether the resonator is stable or unstable (Problem 14.2).

Our stability analysis has assumed perfect mirror reflectivities. In reality, of course, some energy will be taken from the intraresonator laser field because of imperfect mirror reflectivities. We have already noted (Chapter 10) that transmissive output coupling through one (or both) of the mirrors is one such loss mechanism. In addition to such loss mechanisms as output coupling, scattering, or absorption, a laser with an unstable resonator will have a large loss associated with the escape of radiation *past* the mirrors, as indicated by ray tracing as in Figures 14.1*b* and 14.9. Because of this additional loss factor, unstable resonators typically require media with higher gain to sustain laser oscillation. This is not to say that

unstable resonators should always be avoided. On the contrary, unstable resonators offer several advantages for certain high-power lasers (Section 14.13). In more familiar devices such as commercial He–Ne lasers, however, stable resonators are usually employed.

The plane-parallel resonator of Figure 14.1 is not used for practical lasers because it becomes unstable with only slight misalignment of the mirrors. The resonators of most lasers have at least one spherical mirror surface. The hemispherical resonator of Figure 14.8, for instance, is perhaps the most commonly used design for He–Ne lasers.

14.4 THE PARAXIAL WAVE EQUATION

Many important properties of laser resonators are consequences of the wave nature of light. A complete understanding of laser resonators therefore demands a treatment based on Maxwell's equations rather than geometrical rays. In this section we will examine an approximate solution of the Maxwell wave equation that turns out to be very important for laser resonators.

Let us first recall the wave equation (see Section 2.1) for the electric field in vacuum:

$$\nabla^2 E(\mathbf{r}, t) - \frac{1}{c^2}\frac{\partial^2}{\partial t^2} E(\mathbf{r}, t) = 0 \tag{14.4.1}$$

We have written the scalar wave equation instead of the full vector equation. Our treatment will therefore account for diffraction and interference of the radiation inside a resonator, but not for polarization effects. A fully vectorial treatment of laser resonators is very complicated, so fortunately the scalar theory is quite adequate for our purposes. We will be interested in solutions of (14.4.1) of the form

$$E(\mathbf{r}, t) = \mathcal{E}(\mathbf{r})\, e^{-i\omega t} \tag{14.4.2}$$

i.e., monochromatic fields. When this expression is used in the wave equation (14.4.1), we obtain the *Helmholtz equation* for $\mathcal{E}(\mathbf{r})$:

$$\nabla^2 \mathcal{E}(\mathbf{r}) + k^2 \mathcal{E}(\mathbf{r}) = 0 \tag{14.4.3}$$

where

$$k^2 = \omega^2/c^2 \tag{14.4.4}$$

A solution of the Helmholtz equation for $\mathcal{E}(\mathbf{r})$ will provide a monochromatic solution (14.4.2) of the wave equation.

One solution of (14.4.3) is

$$\mathcal{E}(\mathbf{r}) = \mathcal{E}_0\, e^{i\mathbf{k}\cdot\mathbf{r}} \tag{14.4.5}$$

where $\mathcal{E}_0$ is a constant and $\mathbf{k}$ is a vector whose squared magnitude is given by (14.4.4). Such a plane-wave solution was discussed in Chapter 2. It has the same value for all points in any plane normal to $\mathbf{k}$. If we take $\mathbf{k}$ to point in the z direction, for instance, the solution (14.4.5) has the same value ($\mathcal{E}_0 e^{ikz}$) in any plane defined by a constant value of z. Another solution of (14.4.3), valid for all $r \neq 0$, is (Problem 14.3)

$$\mathcal{E}(\mathbf{r}) = \frac{A}{r}\, e^{ikr} \tag{14.4.6}$$

This solution has a constant value on any sphere centered at the origin, and is therefore called a *spherical wave*. This is the form of solution we would associate with a point source at the origin. It represents a (spherical) wave emanating from the origin, with the intensity of the wave (square of $|\mathcal{E}|$) decreasing with distance r according to the inverse square law.

Consider the spherical-wave solution (14.4.6) in the plane ($z = R$) (Figure 14.10). In this plane

$$r = (x^2 + y^2 + R^2)^{1/2} = R\left(1 + \frac{x^2 + y^2}{R^2}\right)^{1/2} \tag{14.4.7}$$

If we restrict ourselves to a small "patch" of observation about the point ($x = 0$, $y = 0$, $z = R$), so that $x^2 + y^2$ is small compared with R^2, then

$$\left(1 + \frac{x^2 + y^2}{R^2}\right)^{1/2} = 1 + \frac{x^2 + y^2}{2R^2} + \cdots \tag{14.4.8}$$

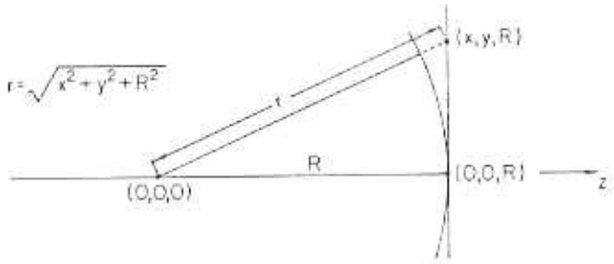

Figure 14.10 Geometry for Eq. (14.4.7).

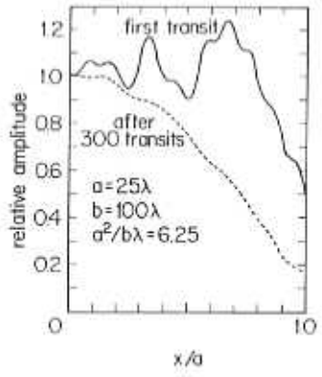

Figure 14.31 Field amplitude distribution computed by Fox and Li for a resonator with flat rectangular mirrors. The mirrors have length 20 in one direction, and are effectively infinite in the other direction. The parameters are such that the Fresnel number $a^2/b\lambda = 6.25$. The iteration process was begun assuming a uniform plane-wave field on one of the mirrors.

obtained is then a solution of (14.12.7), i.e., it is a mode of the resonator. In practice this method will yield straightforwardly only one mode, that of lowest round-trip loss, but certain numerical "tricks" can be employed to obtain higher-loss modes.

Figures 14.31 and 14.32 are reproduced from the original Fox–Li paper. For the example shown, about 300 iterations were necessary for the iterative procedure to converge on a mode of the resonator.

• Equation (14.12.7) may be written in the *operator form*

$$\Gamma \mathcal{E}_0 = \gamma \mathcal{E}_0 \tag{14.12.8}$$

where Γ is the operator corresponding to a round trip through the resonator, i.e., Γ is *defined* by its effect on functions $f(x, y)$:

$$\Gamma f(x, y) = \int\int \hat{K}(x, y; x', y')\, f(x', y')\, dx'\, dy' \tag{14.12.9}$$

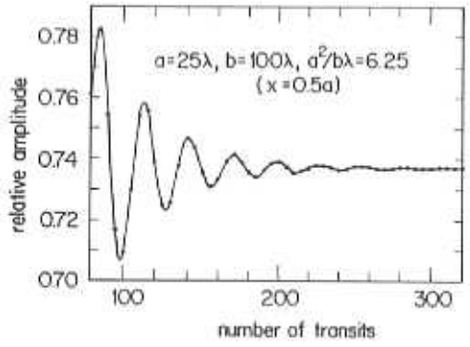

Figure 14.32 Dependence on iteration number of the amplitude at a fixed point on a mirror, as computed by Fox and Li for the case of Figure 14.31.

According to (14.12.8), the modes of a resonator are the eigenfunctions of the operator Γ for the resonator. The number γ is the eigenvalue corresponding to the eigenfunction $\mathcal{E}_0(x, y)$. This sounds a bit like the mathematics of quantum mechanics. Here Γ is generally not a Hermitian operator; for instance, the eigenvalues γ are complex, whereas the eigenvalues of a Hermitian operator are always real. •

14.13 UNSTABLE RESONATORS FOR HIGH-POWER LASERS

Our emphasis on stable laser resonators should not be taken to imply that *unstable* resonators have no practical applications. On the contrary, unstable resonators enjoy certain advantages, and they are essential to the design of many important high-power lasers.

Stable resonators have some drawbacks if one wants to build a high-power device. A major disadvantage is that the modes of stable resonators tend to be concentrated in very thin, needlelike regions within the resonator. Therefore they do not overlap a very large portion of the gain medium, and this obviously presents a problem if high power extraction from the medium is desired. A Gaussian beam mode of a stable resonator, for instance, has a spot size on the order of $(\lambda L/\pi)^{1/2}$ [see Eq. (14.7.21)]. For a CO_2 laser with $\lambda = 10.6\ \mu$m and $L = 1$ m,

$$(\lambda L/\pi)^{1/2} = 1.8 \text{ mm} \tag{14.13.1}$$

a typical sort of beam "size" for Gaussian beam modes of stable resonators.

Unstable resonators, however, typically have much larger mode volumes, and can therefore make better use of the available gain region. Figure 14.33 shows an important practical example of an unstable resonator, the so-called positive-branch (because $g_1 g_2 > 1$) confocal resonator. As indicated, the intracavity field fills a large portion of the cavity, and can be made larger simply by using larger mirrors. The "magnification" M is a function only of the g parameters of the mirrors.

Iterative computations of the Fox–Li type reveal that the modes of unstable resonators like that shown in Figure 14.33 are distinctly non-Gaussian. To a first approximation the lowest-loss mode has a nearly uniform intensity profile on the mirrors. The output beam for the resonator shown in Figure 14.33 is a collimated annular (doughnut-shaped) beam in the *near field* close to the resonator. In the far

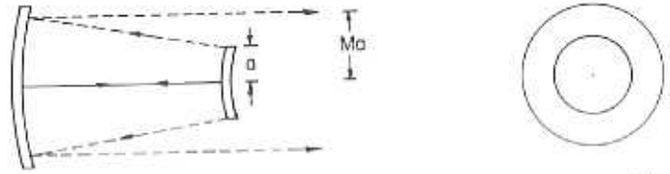

Figure 14.33 A positive-branch ($g_1 g_2 > 1$) confocal unstable resonator. The near-field output is a collimated, annular beam.

field this output beam has a central bright spot on axis. In the limit of large magnification this far field approaches an Airy pattern, with most of the intensity concentrated in the central bright spot.

Unstable resonators offer other advantages in addition to their large mode volumes. For instance, they tend to yield higher output powers when operating on the lowest-loss transverse mode rather than on several (or many) modes. This property is not generally shared by stable-resonator lasers, and it is an important advantage in many applications. In addition, unstable-resonator lasers use *all-reflective optics*. That is, the output does not pass through any mirrors but simply spills around the mirror edges. At high power levels, where mirror damage is an important consideration, the mirrors can often be water-cooled without much difficulty. Obviously the problem of mirror damage and thermal distortion is not so easily surmountable in stable laser resonators employing transmissive output coupling.

The theory of unstable-resonator lasers does not differ in any fundamental way from that of stable-resonator lasers. For this reason, and because stable resonators are more common, we will not consider in any detail the mode characteristics of unstable resonators.

14.14 BESSEL BEAM MODES

In discussing Gaussian beams in Section 14.4 we introduced both the paraxial factorization (14.4.13)

$$\mathcal{E}(\mathbf{r}) = \mathcal{E}_0(\mathbf{r})\, e^{ikz} \tag{14.14.1}$$

and several approximations [recall Eqs. (14.4.14) and (14.4.15)] based on the presumed slow variation of the plane-wave envelope $\mathcal{E}_0(\mathbf{r})$. These are natural steps to take when dealing with beams that spread very little. Surprisingly, they do not lead to a description of the beams that spread the least of all. There is a set of ideally nonspreading beams that are described by Bessel functions rather than by Gaussian–Hermite or Gaussian–Laguerre functions. Although Bessel beam modes have not played any role in laser development so far, we include a description of them here for completeness.

In contrast to the "weak" paraxial factorization (14.14.1), there is also a "strong" factorization. It is introduced by requiring the envelope function $\mathcal{E}_0(\mathbf{r})$ to be completely independent of z. That is, in place of (14.14.1) we write

$$\mathcal{E}(\mathbf{r}) = \mathcal{E}_0(x, y)\, e^{i\beta z} \tag{14.14.2}$$

where we have indicated explicitly the absence of z dependence in the envelope function. In this case, in place of (14.4.19) we find the equation:

$$[\nabla_T^2 + \beta^2]\, \mathcal{E}_0(x, y) = 0 \tag{14.14.3}$$

where ∇_T^2 is the transverse Laplacian defined in (14.4.20). It is easy to check that Eq. (14.14.3), which is the Helmholtz equation in two dimensions rather than three, is an *exact* consequence of the strong paraxial factorization (14.14.2). There are no leftover terms required to be negligible, as there were in the transition from (14.4.16) to (14.4.18).

The solution to the two-dimensional Helmholtz equation was known to be given in terms of Bessel functions at least 50 years before the time of Helmholtz. The solutions are most conveniently expressed in cylindrical coordinates ρ and ϕ:

$$x = \rho \cos \phi \quad \text{and} \quad y = \rho \sin \phi \tag{14.14.4}$$

The solution that is nonsingular at the origin is given by

$$\mathcal{E}_0 \to \mathcal{E}_m(x, y) = A J_m(\alpha\rho)\, e^{im\phi} \tag{14.14.5}$$

where A is a constant and $J_m(x)$ is the mth Bessel function, the same functions introduced in our discussion of FM mode locking in Section 12.10 and shown in Figure 12.13. In order for (14.14.5) to satisfy the two-dimensional Helmholtz equation, and for (14.14.2) to satisfy the full three-dimensional Helmholtz equation (14.4.3), it is only necessary that α and β be connected by the frequency of the light:

$$\alpha^2 + \beta^2 = (\omega/c)^2 \tag{14.14.6}$$

It is clear from (14.14.5) that only the lowest-order solution, the one with $m = 0$, is cylindrically symmetric (independent of ϕ). This is analogous to the situation found earlier with Gaussian–Hermite modes in Section 14.8. Inspection of Figure 12.13 shows that the lowest-order mode also gives the most intense beam near the axis (near $\rho = 0$).

The most remarkable feature of the Bessel mode solutions described here is that they are, in the ideal case, *completely nondiffracting*. To show precisely what this statement means, let us compute the intensity of radiation associated with the general Bessel solution (14.14.5). The physical electric field is the real part of $\mathcal{E}(\mathbf{r})\, e^{-i\omega t}$, which in this case is given by

$$E_m(\mathbf{r}, t) = A J_m(\alpha\rho) \cos(\omega t - kz + m\phi) \tag{14.14.7}$$

The cycle-averaged power flow of the mth Bessel beam mode is then easily seen to be given by

$$I_m(\mathbf{r}, t) = \frac{cc_0}{2} A^2 J_m^2(\alpha\rho) \tag{14.14.8}$$

and this function has the property that it is completely independent of z.